Geochemical Perspectives Letters

No direct contribution of recycled crust in Icelandic basalts

S. Lambart[1,2*]

OPEN ACCESS

doi: 10.7185/geochemlet.1728

Abstract

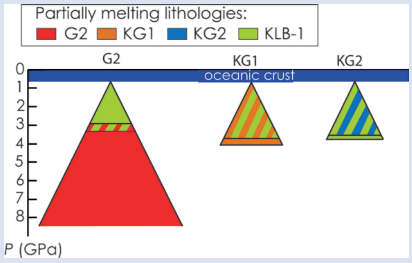

Using Melt-PX to model the decompression melting of a heterogeneous mantle, I investigated the role of major-element composition of the lithologies present in the source on magmatic productivity, and trace element and isotopic melt compositions, independently of the bulk mantle composition. My calculations demonstrate that the volume of magma produced is not significantly affected by the nature of the lithological heterogeneity, but depends on the bulk mantle composition. However, an isochemical bulk mantle can produce contrasting trace element and isotopic melt compositions depending on the major-element compositions of the lithologies present in the source. Results show that the observed crust thickness of the Icelandic rift zones is consistent with about 10 % of recycled crust in the source, but also demonstrate there is no need to involve the contribution of melts derived from a recycled basalt component to explain the compositional variability of the Icelandic basalts in rift zones, and rather advance the contribution of olivine-bearing hybrid lithologies formed by solid-state reactions between the recycled crust and the peridotite.

Received 2 April 2017 | Accepted 6 June 2017 | Published 12 July 2017

Introduction

It is widely accepted that the compositional spectrum of Icelandic lavas requires the presence of at least two components in the mantle source (*e.g.*, Thirlwall *et al.*, 2004, 2006; Sobolev *et al.*, 2007; Brown and Lesher, 2014). However, the nature of these components is still debated and two end-member models have been suggested: while trace element and isotopic analyses of Icelandic lavas seem to suggest the presence of two distinct lithologies in the form of pyroxenite and peridotite (*e.g.*, Kokfelt *et al.*, 2006; Koornneef *et al.*, 2012; Brown and Lesher, 2014), major-element compositions and olivine chemistry suggest a peridotite mantle composed of more or less re-fertilised domains by reaction with the recycling material (Shorttle and Maclennan, 2011; Herzberg *et al.*, 2016). Using a quantitative melting model for the adiabatic decompression of a multi-lithological source, I show that trace element and isotopic compositions of the Icelandic basalt suite can be reproduced without involving the contribution of melts derived from the recycled basalt component in the mantle source.

Strategy

Lambart *et al.* (2016) demonstrated that the final extent of melting and the mean melting pressure of the potential lithologies present in the mantle sources are strong functions of their major element composition. Hence, the same mantle bulk composition may melt differently and produce different trace element and isotopic melt compositions depending on the specific lithologies that are present and make up the bulk composition. To test this hypothesis, I considered a bulk mantle composition corresponding to 10 % recycled oceanic crust G2 + 90 % peridotite KLB-1 (Bulk1 in Table S-1) and compared the melting behaviour during adiabatic decompression at T_P = 1480 °C of three different heterogeneity distributions in the mantle: G2-, KG1- and KG2-configurations. In the "G2-configuration", the two distinct lithologies are the MORB-like type eclogite G2 (Pertermann and Hirschmann, 2002) and the peridotite KBL-1 (Hirose and Kushiro, 1993). To model the KG1- and KG2-configurations, I considered a mantle containing 20 % lithology KG1 and 80 % peridotite KLB-1, and a mantle containing 30 % lithology KG2 and 70 % peridotite KLB-1, respectively. Because KG1 and KG2 (Kogiso *et al.*, 1998) are two compositions produced by mixing 1/2 G2 and 1/2 KLB-1, and 1/3 G2 and 2/3 KLB-1, respectively, all three mantle configurations are isochemical (Bulk 1 in Table S-1). In the three configurations, the two lithologies present in the source are chemically isolated but in thermal equilibrium.

Using Melt-PX (Lambart *et al.*, 2016), I modelled the decompression melting of these three mantle configurations for a potential temperature T_P = 1480 °C and calculated the trace element and isotopic compositions of the accumulated melts for complete mixing of melts from the two mantle components integrated over the melting column (Supplementary Information). Similar heterogeneous melting models have been described in the literature but, unlike those presented here, the melting behaviours of the different components were

1. Department of Earth and Planetary Sciences, University of California Davis, One Shields Avenue, Davis, California 95616, USA
2. School of Earth and Ocean Sciences, Cardiff University, CF10 3AT Cardiff, UK
* Corresponding author (email: sarahlambart@yahoo.fr)

arbitrarily chosen (*e.g.*, Ito and Mahoney, 2005; Stracke and Bourdon, 2009; Waters *et al.*, 2011), the *F versus T* relationships were calculated with pMELTS (*e.g.*, Rudge *et al.*, 2013; Sims *et al.*, 2013) that strongly overestimates the size of melting interval of mantle lithologies and especially pyroxenites, by both overestimating the liquidus temperature and underestimating the solidus temperature (Lambart *et al.*, 2016), and/or the thermal interactions between components were not taken into account (*e.g.*, Koornneef *et al.*, 2012). This study presents the first quantitative calculations taking into account the effect of the major element composition on the melting behaviours of the lithologies present in the source and on trace element and isotopic compositions of the magmas produced.

Results

Results of the calculations with Melt-PX are illustrated in Figure 1. The mantle melting behaviour is much contrasted between the three configurations. In the G2-configuration, the pyroxenite component starts to melt at very high pressure (~8.7 GPa), but rapidly stops soon after the peridotite crosses its solidus (Fig. 1a). This phenomenon occurs because the adiabatic melting path is steeper than the solidus of G2 residue once the peridotite solidus is crossed (Fig. S-1; Lambart *et al.*, 2016). Hence, partial melts generated along the adiabatic path are initially derived from the pyroxenite alone; once the peridotite starts to melt, the fraction of G2-derived melt in the aggregated liquid decreases by dilution with decreasing pressure (Fig. 1b). Unlike G2, lithology KG1 starts to melt just before the peridotite and, despite a drop of melt productivity when the peridotite solidus is crossed (Fig. S-2), both KG1 and KLB-1 continue to melt simultaneously. Finally, KG2 starts to melt after the peridotite but the melt productivity of KG2 is higher than the one of KLB-1 (Fig. S-3) and the fraction of KG2-derived liquid in the aggregated partial melt progressively increases with decreasing pressure (Fig. 1b). Despite these contrasting behaviours, the magmatic productivity and consequently the oceanic crust thickness produced in the three configurations are very similar with 21.8, 22.3 and 22.0 km for G2-, KG1- and KG2-configuration, respectively.

The trace element and isotopic compositions of the pooled melts for the three configurations along the adiabatic path are presented in Figure 2. Stracke and Bourdon (2009) demonstrated that trace element ratios involving a moderately incompatible element (*e.g.*, La/Sm, La/Yb, Hf/Yb) are dominantly influenced by the melting process. In fact La/Sm *vs.* La/Yb variations (Fig. 2a) show similar trends in the three configurations. On the contrary, highly incompatible element ratios, such as Ba/Th (Fig. 2b), do not vary significantly with progressive melting and differences between the ratios reflect differences in the source components. The three configurations show contrasting trends in the Sr-Nd isotopic space (Fig. 2d). Both G2- and KG1-configurations produced melts that become progressively less radiogenic due to the decrease of the recycled component contribution in the pooled melt along the adiabatic path (Fig. 1b). Interestingly, the range of isotopic compositions produced in G2-configuration is much smaller than the one produced in KG1-configuration. KG2-configuration produces melts that become increasingly radiogenic with decreasing pressure due to the increase of recycled crust contribution along the adiabatic path (Fig. 1b). Finally, correlations between trace element ratios and isotopic ratios show very distinctive trends for the three configurations (Fig. 2e-f). In the G2-configuration, the $^{143}Nd/^{144}Nd$ of the pooled melt stays constant as long as only G2 is melting, while the La/Yb ratio decreases with increasing *F*. When the peridotite starts to melt, G2 has reached 57 wt. % melting and the accumulated melt is much depleted in incompatible trace elements. The addition of an isotopically depleted peridotite partial melt results in a shift of the pooled liquid isotopic composition, while the La/Yb ratio stays relatively constant (Fig. 2e). In the KG1-configuration, KG1 only reached 13 wt. % melting at the onset of the peridotite melting. Hence, the La/Yb ratio continues to decrease with the increasing melting degree of KG1 while the addition

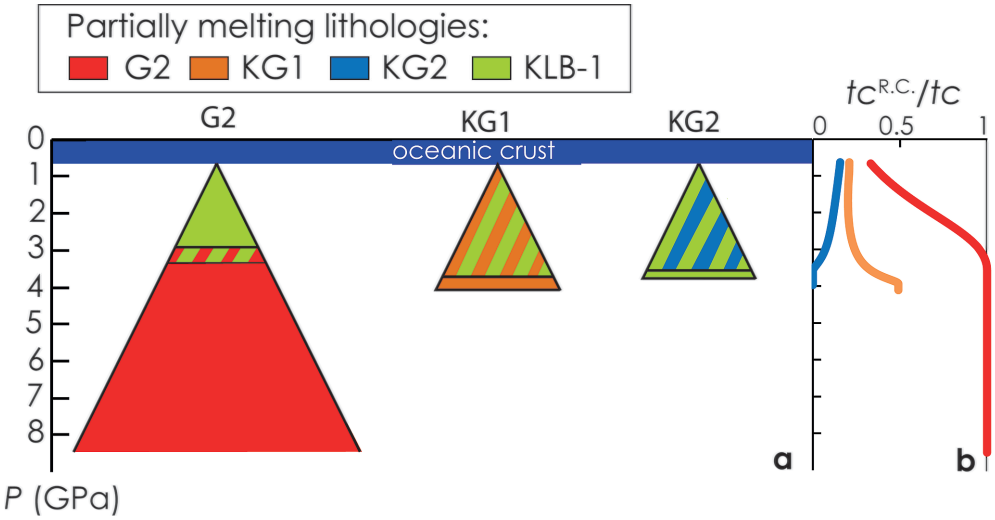

Figure 1 **(a)** Representation of the melting column in the three configurations. Colours show the lithologies that are partially melting at a given pressure. **(b)** Contribution of the recycled crust ($tc^{R.C.}/tc$) to the melt production as functions of the pressure along the adiabatic path in G2- (red), KG1- (orange) and KG2- (blue) configurations. The contribution of the recycled crust is assumed to be equal to the contribution of G2, to half of the contibution of KG1 and to one third of the contribution of KG2, in the respective configurations.

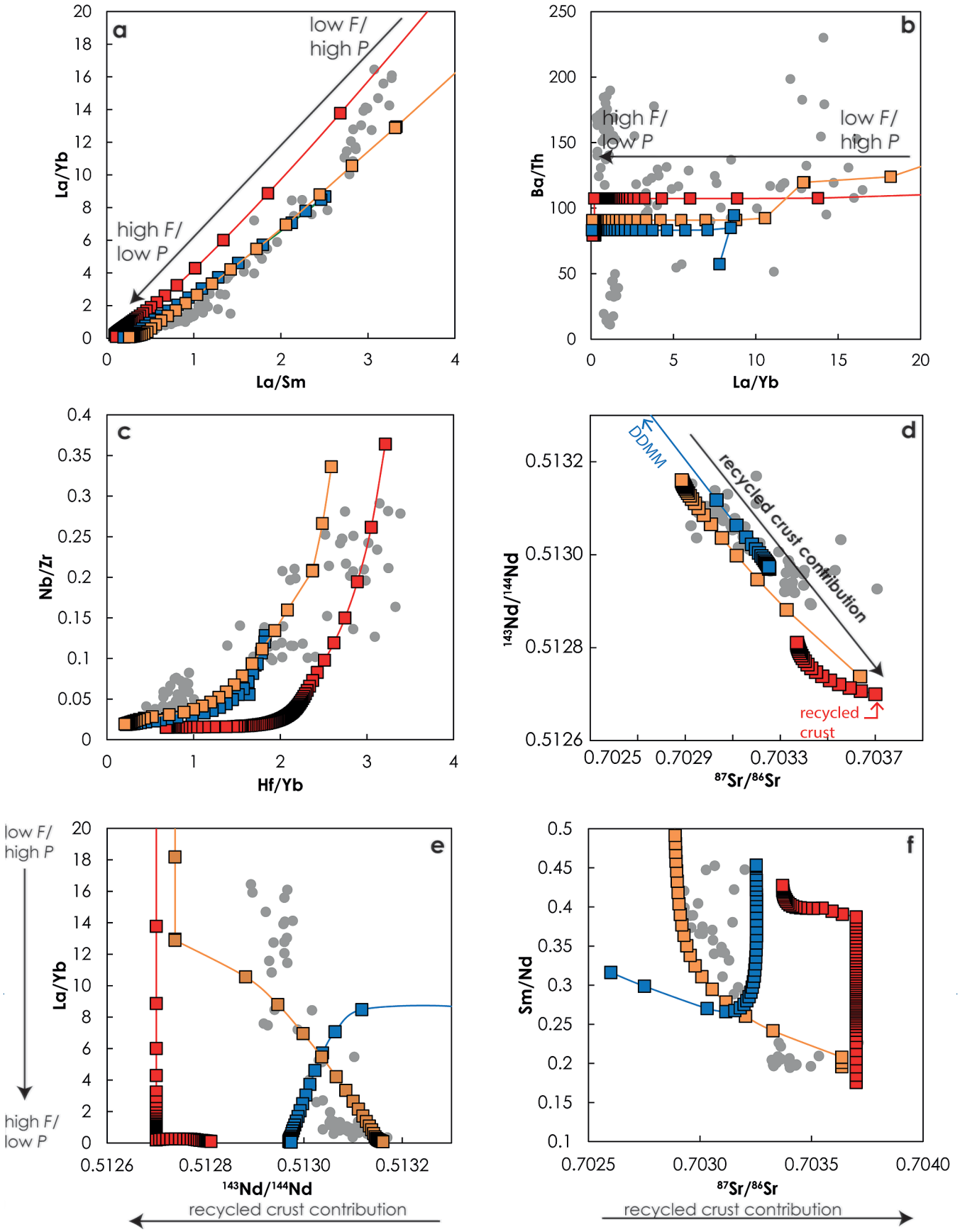

Figure 2 Compositions of the aggregated melts produced over the melting column in G2- (red), KG1- (orange) and KG2- (blue) configurations. Grey dots are the compositions of Icelandic basalts with MgO contents between 9.5 and 17 wt. % from the Northern Volcanic zone, the Reykjanes Peninsula, the Snaefellsnes area and the South Eastern Volcanic Zone (GEOROC). Detailed explanations of the calculations are given in the Supplementary Information.

of peridotite melt increases the isotopic ratio $^{143}Nd/^{144}Nd$ of the pooled melt. Finally, in the KG2-configuration, the peridotite starts to melt before KG2 and the first degree melt is a peridotite liquid at 3.6 GPa (Figs. 1, S-5). Soon after, the solidus of KG2 is crossed and the aggregated melt becomes more isotopically enriched due to the addition of KG2-derived melt (the $^{143}Nd/^{144}Nd$ ratio decreases and the $^{86}Sr/^{87}Sr$ ratio increases with decreasing pressure; Fig. 2e-f).

Implications for the Nature of the Mantle Heterogeneity Beneath Iceland

Several studies have questioned the necessity to involve the direct contribution of melts from the recycled component to the magmatic production beneath Iceland (Shorttle and MacLennan, 2011; Herzberg *et al.*, 2016). On Figure 2, I compared the calculated trends with the observed variation in Icelandic basalts produced in the rift zones at the coasts (GEOROC database). Consistent with the calculations, magma production in this context is thought to reflect a passive plate spreading alone (Brown and Lesher, 2014, Shorttle *et al.*, 2014) and T_P = 1480 °C is in agreement with the most recent estimated potential mantle temperature beneath Iceland (Matthews *et al.,* 2016). Calculated crust thicknesses are in fact similar to the estimated crustal thicknesses in Iceland's rift zones (Darbyshire *et al.,* 2000). In addition, these calculations suggest that in the context of passive melting regime, the volume of magma produced is relatively independent of the nature of the lithological heterogeneity, but is mainly controlled by the mantle potential temperature (Lambart *et al.*, 2016) and the bulk mantle composition. Calculations show that the trace element – isotope systematics are mostly controlled by the pressure difference between the onset of melting of the lithologies present in the source (Stracke and Bourdon, 2009). Overall, the trace element and isotopic systematics of Icelandic basalts are well reproduced by the melting of a mantle containing 20 % KG1. In detail, the trace element compositions of Icelandic basalts become more depleted with increasing $^{143}Nd/^{144}Nd$ ratios (Fig. 2e) and decreasing $^{87}Sr/^{86}Sr$ (Fig. 2f). In other words, the progressive depletion of the Icelandic melts with increasing extent of melting indicates that the enriched component becomes progressively diluted with the peridotite component. This is only possible if the enriched component has a lower solidus temperature compared to the depleted component, in agreement with Sims *et al.* (2013). Moreover, Figure 2 suggests that a small difference in solidus temperature of the enriched and depleted components is required to reproduce the co-variations between trace element and isotopic ratios, especially those involving highly incompatible elements over moderately incompatible elements (Fig. 2e-f). Otherwise, for large solidus temperature differences between the two components, such as in G2-configuration, the enriched component will undergo large degree of melting before onset of the peridotite melting resulting in insufficient enrichment of melts in highly incompatible elements. Hence, by using Melt-PX to model the melting behaviour of the mantle components, this study provides quantitative constraints on the melting behaviour, and consequently on the major-element composition, of the lithologies present in the source.

It could be argued that the absolute positions of the compositional trends along the isotopic ratio axes in Figure 2e-f depend on the isotopic compositions chosen for the peridotite and the recycled components (Table S-1). For the peridotite component, I chose the isotopic composition of the most depleted end of the MORB field reported by Salters and Stracke (2004). In fact, unradiogenic Pb isotopic compositions, Nd and Hf isotope systems and trace element systematics of Icelandic basalts have all been used to validate the presence of a distinct depleted endmember for the Iceland plume (*e.g.*, Thirlwall *et al.*, 2004, 2006; Shorttle *et al.*, 2014 and references therein). For the recycled crustal component, I chose a 2 Ga recycled crust (*e.g.*, Chauvel and Hémond, 2000; Kokfelt *et al.,* 2006). However, the age of the recycled component in the basalt source of Iceland is highly debated and could be younger by up to an order of magnitude (Halldórsson *et al.,* 2016). A younger recycled material will have a lower content of radiogenic isotopes and consequently trends in Figure 2e-f will be shifted toward higher $^{143}Nd/^{144}Nd$ ratios and lower the $^{87}Sr/^{86}Sr$ ratios. For instance, the range of Nd isotopic compositions displayed by the Icelandic basalt (Fig. 2d) could be reproduced in the G2-configuration by varying the age of the recycled component from 1.7 to 0.5 Ga, but would not explain the co-variations between trace element and isotopic ratios (Fig. 2e). In the following section I provide additional constraints on the nature of the mantle heterogeneity beneath Iceland by looking at the implications of these observations for melt extraction mechanisms.

Constraints from Melt Extraction

It was shown in the preceding section that (1) the compositional variability of Icelandic basalt requires at least two different mantle components with different radiogenic isotopic compositions, (2) the most radiogenic component should have the lowest solidus temperature (as in G2- or KG1-configurations), and equally importantly (3) the pooled melts need to be extracted at different depths along the adiabatic path, in agreement with the conclusions of Stracke and Bourdon (2009). This last observation implies an efficient melt extraction mechanism capable of sampling relatively low degree partial melts without significant interaction with the mantle. In the G2-configuration, the peridotite mostly stays subsolidus during the melting of the pyroxenite (Fig. 1a) and the highest La/Yb (>12) and La/Sm (>3) ratios displayed by the Icelandic basalts (Fig. 2a) are produced at P > 8.3 GPa (Fig. S-6). Hence, the G2-configuration requires the unlikely scenario of the circulation of a very silica-rich (Fig. S-7) low-degree melt into a subsolidus peridotite mantle from 8.3 GPa to 3.1 GPa (the onset of peridotite melting) and without significant melt-rock interaction. In the KG1-configuration, the peridotite starts to melt soon after the enriched component (Fig. 1a) and the highest La/Yb and La/Sm ratios are produced at P > 3.4 GPa, *i.e.* by the melting of the KG1 component only. However, unlike G2, KG1 produces melts with major element compositions very similar to peridotite melts (Fig. S-7). This small compositional contrast will result in limited reactivity between KG1-derived melt and peridotite, favourable to the preservation of their trace element signature (Lambart *et al.,* 2012). Finally, it should be noted that, in the G2-configuration, the entire range of trace element compositions observed in Icelandic basalts is produced by the melting of the pyroxenite G2 while the peridotite component stays subsolidus. Lambart *et al.* (2012) showed that migration of melts in a subsolidus mantle results in a strong consumption of the melt. On the contrary, melt extraction is facilitated when the surrounding mantle is partially melted, as in the KG1-configuration in which, with the exception of the most enriched basalt compositions (La/Yb > 12 and La/Sm > 3), both KG1 and KLB-1 are contributing to the pooled melts (Fig. S-6).

Solid-State Reaction Versus Melt–Rock Reaction

Calculations presented above resolve an ambiguity that has arisen in the literature, between the need for the direct contribution of melts from recycled basaltic lithologies, *versus* the manifestation of their presence through re-fertilised hybrid lithologies, and demonstrate that hybrid lithologies can be an important contributor to lithological diversity in the mantle. However, these hybrid lithologies could be formed either by solid-state reaction (*i.e.* homogeneous mixing and phase equilibration between the solid recycled crust and the solid peridotite) or by melt-rock reaction, in which melts derived from the recycled crust react with the peridotite to form an olivine-free secondary pyroxenite, such as Px-1 (Sobolev *et al.*, 2007). Because KG1 and Px-1 have similar solidus and melting curves (Fig. S-8; Lambart *et al.*, 2016), the trace element – isotope systematics that would be produced by an isochemical bulk mantle containing Px-1 would be very similar to the one produced by the KG1-configuration and would not lead to the discrimination between both models. Similarly, both models can reproduce the high nickel content of primitive Icelandic olivine (Fig. S-9). However, one major difference between these two models, is the major-element composition of the hybrid lithology and consequently, of the derived melts produced by these lithologies. In fact, olivine-free secondary pyroxenites produced melts with similar silica content to G2-derived melts (Fig. S-7). As mentioned above, such melts are likely to react with the surrounding peridotite to produce pyroxenes and dissolve olivine and, consequently, are less likely to preserve their compositional signature.

In summary, this study supports the fact that two distinct mantle components are required to explain the compositional diversity of Icelandic basalts with the most radiogenic component being the most fusible, but also demonstrates that the direct contribution of the melts derived from the recycled crust cannot explain the trace element – isotope systematics of Icelandic basalt, and rather advances the polybaric melting of various olivine-bearing lithologies, likely produced by solid-state interactions between the recycled crust and the peridotite.

Acknowledgements

This study has benefited from discussions with Mike Baker and Ed Stolper. This work was supported by the National Science Foundation grant EAR-1551442 and the European Union's Horizon 2020 research and innovation programme under the Marie Skłodowska-Curie grant agreement No. 663830. Two anonymous reviewers are thanked for their helpful suggestions.

Editor: Graham Pearson

Additional Information

Supplementary Information accompanies this letter at www.geochemicalperspectivesletters.org/article1728

Reprints and permission information are available online at http://www.geochemicalperspectivesletters.org/copyright-and-permissions

Cite this letter as: Lambart, S. (2017) No direct contribution of recycled crust in Icelandic basalts. *Geochem. Persp. Let.* 4, 7-12.

References

Brown, E.L., Lesher, C.E. (2014) North Atlantic magmatism controlled by temperature, mantle composition and buoyancy. *Nature Geoscience* 7, 820–824.

Chauvel, C., Hémond, C. (2000) Melting of a complete section of recycled oceanic crust: Trace element and Pb isotopic evidence from Iceland. *Geochemistry, Geophysics, Geosystems* 1, 1001.

Darbyshire, F.A., White, R.S., Priestley, K.F. (2000) Structure of the crust and uppermost mantle of Iceland from a combined seismic and gravity study. *Earth and Planetary Science Letters* 181, 409–428.

Halldórsson, S.A., Hilton, D.R., Barry, P.H., Füri, E., Grönvold, K. (2016) Recycling of crustal material by the Iceland mantle plume: New evidence from nitrogen elemental and isotope systematics of subglacial basalts. *Geochimica et Cosmochimica Acta* 176, 206–226.

Herzberg, C., Vidito, C., Starkey, N.A. (2016) Nickel-cobalt contents of olivine record origins of mantle peridotite and related rocks. *American Mineralogist* 101, 1952–1966.

Hirose, K., Kushiro, I. (1993) Partial melting of dry peridotites at high pressures: Determiantion of compositions of melts segregated from peridotite using aggregates of diamond. *Earth and Planetary Science Letters* 114, 477–489.

Ito, G., Mahoney, J.J. (2005) Flow and melting of a heterogeneous mantle: 1. Method and importance to the geochemistry of ocean island and mid-ocean ridge basalts. *Earth and Planetary Science Letters* 230, 29–46.

Kogiso, T., Hirose, K., Takahashi, E. (1998) Melting experiments on homogeneous mixtures of peridotite and basalt: application to the genesis of ocean island basalts. *Earth and Planetary Science Letters* 162, 45–61.

Kokfelt, T.F., Hoernle, K., Hauff, F., Fiebig, J., Werner R., Garbe-Schönberg, D. (2006) Combined Trace Element and Pb-Nd–Sr-O Isotope Evidence for Recycled Oceanic Crust (Upper and Lower) in the Iceland Mantle Plume. *Journal of Petrology 47,* 1705–1749.

Koornneef, J.M., Stracke, A., Bourdon, B., Meier, M.A., Jochum, K.P., Stoll, B., Grönvold, K. (2012) Melting of a Two-component Source beneath Iceland. *Journal of Petrology* 53, 127–157.

Lambart, S., Laporte, D., Provost, A., Schiano, P. (2012) Fate of pyroxenite-derived melts in the peridotitic mantle: Thermodynamical and experimental constraints. *Journal of Petrology* 53, 451–476.

Lambart, S., Baker, M.B., Stolper, E.M. (2016) The role of pyroxenite in basalt genesis: Melt-PX, a melting parameterization for mantle pyroxenites between 0.9 and 5GPa. *Journal of Geophysical Research: Solid Earth* 121, doi:10.1002/2015JB012762.

Matthews, S., Shorttle, O., Maclennan, J. (2016) The temperature of the Icelandic mantle from olivine-spinel aluminum exchange thermometry. *Geochemistry, Geophysics, Geosystems* 17, 4725–4752.

Pertermann, M., Hirschmann, M.M. (2003) Anhydrous Partial Melting Experiments on MORB-like Eclogite: Phase Relations, Phase Compositions and Mineral–Melt Partitioning of Major Elements at 2–3 GPa. *Journal of Petrology* 44, 2173–2201.

Rudge, J.F., Maclennan, J., Stracke, A. (2013) The geochemical consequences of mixing melts from a heterogeneous mantle. *Geochimica et Cosmochimica Acta* 114, 112–143.

Salters, V.J.M., Stracke, A. (2004) Composition of the depleted mantle. *Geochemistry, Geophysics, Geosystems* 5, Q05004, doi:10.1029/2003GC000597.

Shorttle, O., Maclennan, J. (2011) Compositional trends of Icelandic basalts: Implications for short-length scale lithological heterogeneity in mantle plumes. *Geochemistry, Geophysics, Geosystems* 12, Q11008, doi:10.1029/2011GC003748.

Shorttle, O., Maclennan, J., Lambart, S. (2014) Quantifying lithological variability in the mantle. *Earth and Planetary Science Letters* 395, 24–40.

Sims, K.W.W., Maclennan, J., Blichert-Toft, J., Mervine, E.M., Blusztajn, J., Grönvold, K. (2013) Short length scale mantle heterogeneity beneath Iceland probed by glacial modulation of melting. *Earth and Planetary Science Letters* 379, 146–157.

Sobolev, A.V., Hofmann, A.W., Kuzmin, D.V., Yaxley, G.M., Arndt, N.T., Chung, S.L., Danyushevsky, L.V., Elliott, T., Frey, F.A., Garcia, M.O., Gurenko, A.A., Kamenetsky, V.S., Kerr, A.C., Krivolutskaya, N.A., Matvienkov, V.V., Nikogosian, I.K., Rocholl, A., Sigurdsson, I.A., Sushchevskaya, N.M., Teklay, M. (2007) The amount of recycled crust in sources of mantle-derived melts. *Science* 316, 412–417.

Stracke, A., Bourdon, B. (2009) The importance of melt extraction for tracing mantle heterogeneity. *Geochimica et Cosmochimica Acta* 73, 218–238.

Thirlwall, M.F., Gee, M.A.M., Taylor, R.N., Murton, B.J. (2004) Mantle components in Iceland and adjacent ridges investigated using double-spike Pb isotope ratios. *Geochimica et Cosmochimica Acta* 68, 361–386.

Thirlwall, M.F., Gee, M.A.M., Lowry, D., Mattey, D.P., Murton, B.J., Taylor, R.N. (2006) Low $\delta^{18}O$ in the Icelandic mantle and its origins: evidence from Reykjanes ridge and Icelandic lavas. *Geochimica et Cosmochimica Acta* 70, 993–1019.

Waters, C.L., Sims, K.W.W., Perfit, M.R., Blichert-Toft, J., Blusztajn, J. (2011) Perspective on the Genesis of E-MORB from Chemical and Isotopic Heterogeneity at 9-10°N East Pacific Rise. *Journal of Petrology* 52, 565–602.

Geochemical Perspectives Letters

No direct contribution of recycled crust in Icelandic basalts

S. Lambart[1,2*]

Supplementary Information

The Supplementary Information includes:

- Methods and Extended Discussion
- Supplementary Information References
- Figures S-1 to S-9
- Tables S-1 to S-3

Methods and Extended Discussion

Melting and melt mixing of a heterogeneous source

It is widely accepted that MORBs are mixes of melts from all depths in the melting column (*e.g.*, Klein and Langmuir, 1987; Langmuir *et al.*, 1992). In these calculations, I assumed that this dynamic model can be applied to the rift zones in Iceland where the melting regime is similar to the melting regime beneath mid-ocean ridges (Brown and Lesher, 2014, Shorttle *et al.*, 2014). In fact, correlations between trace element and isotope compositions in Icelandic basalts (Fig. 2e-f in the main text) indicate that the melting process and sampling of source heterogeneity are intrinsically related. In addition, melt extraction without continuous equilibration with the ambient mantle is required to explain the compositional variability observed in single flow (Maclennan *et al.*, 2003) and the preserved U-series disequilibria (Koornneef *et al.*, 2012a and references therein). High-porosity melt channels are good candidates for promoting melt mixing between the two source components while providing an efficient melt extraction process (Kelemen *et al.*, 1997). Moreover, Weatherley and Katz (2016) recently suggested that channelised flow can be a consequence of melting of a heterogeneous mantle.

Methods

Melt-PX calculations. I used Melt-PX (Lambart *et al.*, 2016) to model the decompression melting of the three mantle configurations. In this model, melting and decompression are assumed to occur isentropically in a passive triangular melting regime (White *et al.*, 1992), the various lithologies are in thermal equilibrium but chemically isolated, and melts from each lithology are mixed continuously along the melting column. Calculations have been performed for T_P = 1480 °C and with an initial clinopyroxene mode in the peridotite of 15 %. At this T_P, along an adiabatic decompression path, G2 starts to melt at much higher pressure than the fertile peridotite and stops soon after the peridotite solidus is crossed (Fig. S-1). This phenomenon occurs because, once the peridotite solidus is crossed, too much latent heat is consumed by the large fraction of peridotite undergoing melting for the G2 residue to stay above its solidus during further ascent (Phipps Morgan, 2001; Lambart *et al.*, 2016). In other words, G2 stops melting because, following the onset of KLB-1 melting, the mantle moves below (or parallel to) G2's melt depleted solidus. KG1 starts to melt just before the peridotite and continues to melt with the peridotite (Fig. S-2). Finally, KG2 starts to melt after the fertile peridotite (Fig. S-3). Calculations were stopped when the mantle column had upwelled to the base of the crust, *i.e.* when the pressure at the base of the crust, $P_c = P$.

pMELTS calculations. pMELTS (Ghiorso *et al.*, 2002) is not suitable for estimating pyroxenite melt fractions as a function of *P* and *T*, but can provide reasonable estimations of the phase assemblage at each pressure step (Lambart *et al.*, 2016). Hence, I used pMELTS to calculate the residual phase assemblages along the adiabatic decompression path calculated with Melt-PX (Lambart *et al.*, 2016). At each *P-F* condition, I calculated the residual phase assemblage using the isobaric batch melting mode. For each component, calculations start at $P_{F=1\%}$ and are repeated every 0.01 GPa pressure interval. Note that while trace element calculations attempt to simulate a near-fractional melting through a series of iterative batch melting calculations, the major element composition of each component is kept constant in the calculations. However, the melting regime (fractional *vs.* batch) does not significantly affect the phase assemblage (Fig. S-4), and consequently will not affect significantly the trace element composition of the melt at each pressure increment. To perform the pMELTS calculations, I took the same choices and constraints as Lambart *et al.* (2016): (1) calculations were made at f_{O_2} = FMQ – 1 (*i.e.* the fayalite-magnetite-quartz buffer minus one log unit), (2) I used the corrected version of the garnet model (Berman and Koziol, 1991) and (3) Cr_2O_3 and MnO were not included in the calculations.

1. Department of Earth and Planetary Sciences, University of California Davis, One Shields Avenue, Davis, California 95616, USA
2. School of Earth and Ocean Sciences, Cardiff University, CF10 3AT Cardiff, UK
* Corresponding author (email: sarahlambart@yahoo.fr)

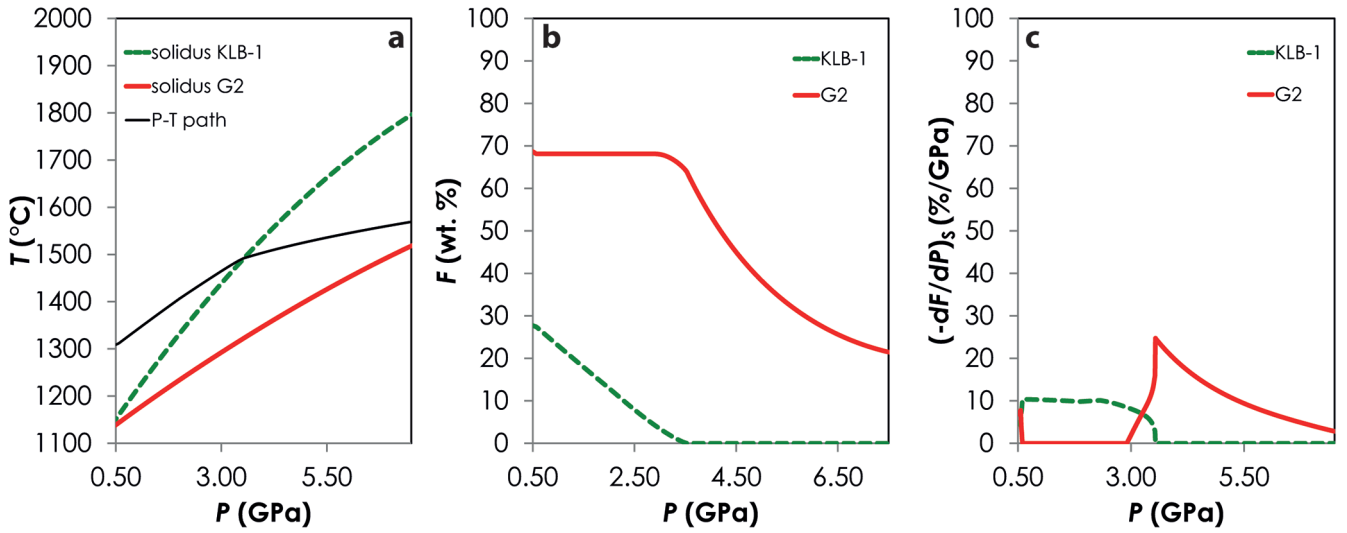

Figure S-1 Results of the Melt-PX calculations for the G2-configuration at a potential temperature of 1480 °C. **(a)** Pressure-temperature path for the column of mantle undergoing isentropic decompression (black line). The solid red and the dashed green lines are the solidi of G2 and KLB-1, respectively. **(b-c)** Extent of the melting **(b)** and melt productivity **(c)** of G2 (solid red line) and KLB-1 (dashed green line) along the adiabatic path.

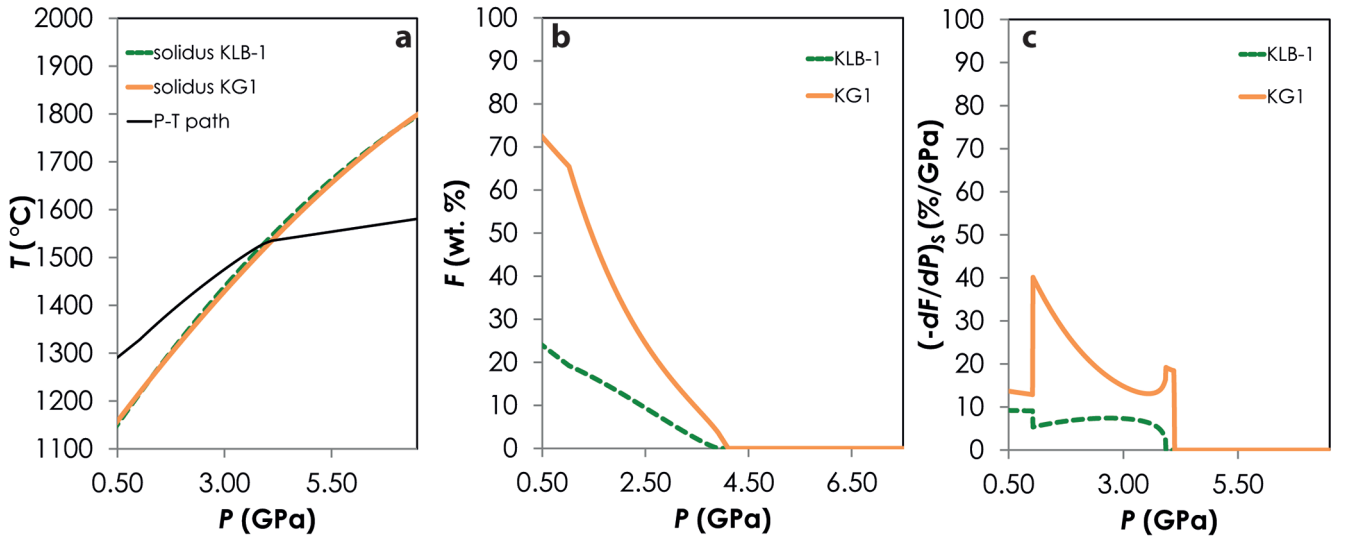

Figure S-2 Results of the Melt-PX calculations for the KG1-configuration at a potential temperature of 1480 °C. **(a)** Pressure-temperature path for the column of mantle undergoing isentropic decompression (black line). The solid orange and the dashed green lines are the solidi of KG1 and KLB-1, respectively. **(b-c)** Extent of the melting **(b)** and melt productivity **(c)** of KG1 (solid orange line) and KLB-1 (dashed green line) along the adiabatic path.

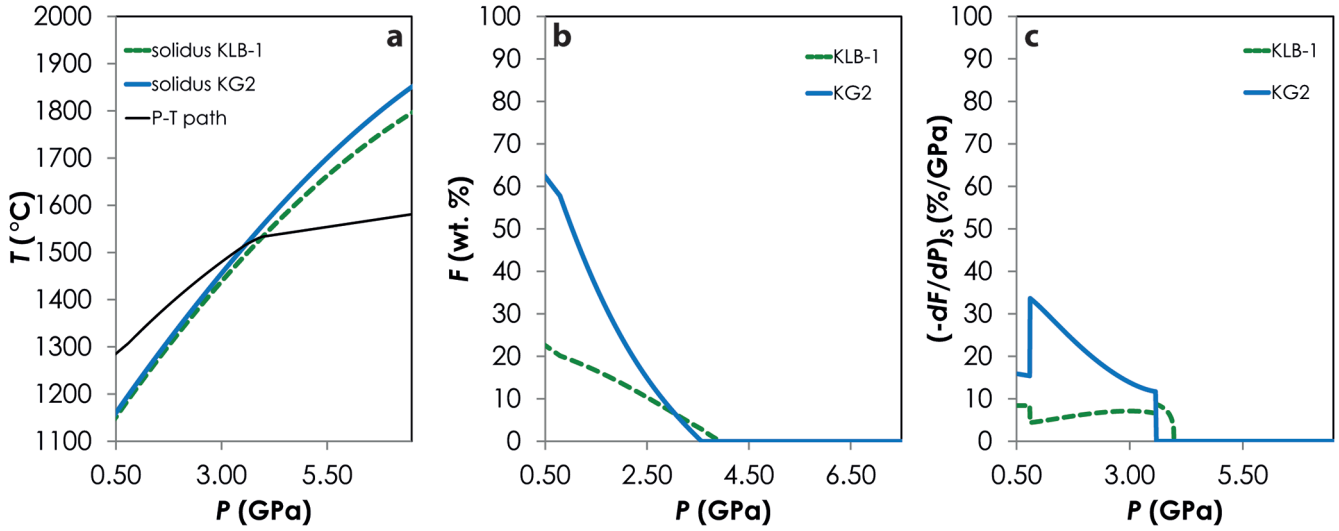

Figure S-3 Results of the Melt-PX calculations for the KG2-configuration at a potential temperature of 1480 °C. **(a)** Pressure-temperature path for the column of mantle undergoing isentropic decompression (black line). The solid blue and the dashed green lines are the solidi of KG1 and KLB-1, respectively. **(b-c)** Extent of the melting **(b)** and melt productivity **(c)** of KG1 (solid blue line) and KLB-1 (dashed green line) along the adiabatic path.

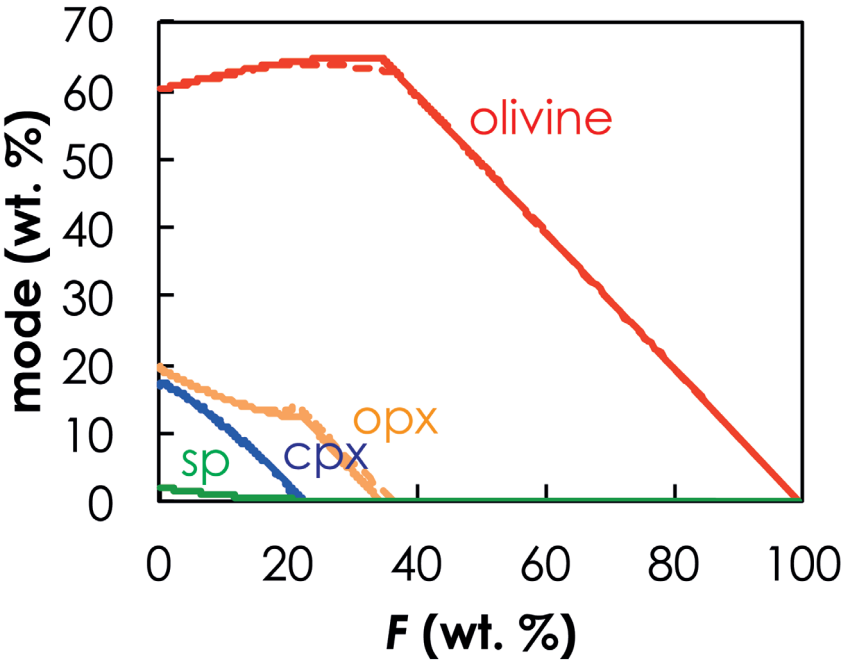

Figure S-4 Evolution of the solid phase modes for the composition KLB-1 (Hirose and Kushiro, 1993) as a function of the proportion of melt during batch melting (solid lines) and continuous melting (dashed lines). The threshold for melt segregation in the continuous melting calculations is 1 %. Calculations were performed at 1 GPa using the thermodynamic model pMELTS (Ghiorso *et al.*, 2002) and the alphaMELTS front-end (Smith and Asimow, 2005). Olivine: red; orthopyroxene (opx): orange; clinopyroxene (cpx): blue; spinel (sp): green.

Trace element calculations. For the recycled component G2, I used the trace element and isotopic composition of the recycled component in Koornneef *et al.* (2012b). The trace element composition corresponds to a mix between E-MORB 1312-47 (Sun *et al.*, 2008) and average gabbro 735B (Hart *et al.*, 1999) in a 1:1 ratio. The isotopic composition corresponds to a 2 Ga recycled oceanic crust altered by sea water and modified during the subduction process by dehydration (Stracke *et al.*, 2003). The peridotite component has the trace element composition of the depleted DMM in Workman and Hart (2005) and the isotopic composition of the Extreme D-MORB in Salters and Stracke (2004).

Continuous melting is simulated by incremental 'dynamic melting'; that is, by small steps of batch melting while keeping a small melt fraction residual.

(1) Incremental melts produced by each lithology.

I assumed that the melt formed at $F = 1$ % is in equilibrium with the residual solid phases.

$$Cl^A\left(P_{F=1\%}\right)=\frac{C_0^A}{0.01+D_0^A\left(P_{F=1\%}\right)\cdot\left(1-0.01\right)} \quad \text{Eq. S-1}$$

$C_0{}^A$ is the initial bulk trace element composition of the lithology A. $D_0{}^A$ is the bulk partition coefficient and is calculated using the set of partition coefficients provided in alphaMELTS (Smith and Asimow, 2005) and the phase assemblage obtained with pMELTS at $P_{F=1\%} - F = 1$ % condition along the adiabatic decompression path previously calculated with Melt-PX (Lambart *et al.*, 2016). The primitive mantle normalised trace element patterns for the first-degree melts produced in the three configurations are plotted in Figure S-5.

Then, the bulk trace element composition is recalculated by extracting the first-degree melt.

$$C_0^A\left(P_{F=1\%}-dP\right)=\frac{C_0^A-0.01\cdot Cl^A\left(P_{F=1\%}\right)}{\left(1-0.01\right)} \quad \text{Eq. S-2}$$

These operations are repeated for the next pressure increment $-dP$:

$$Cl^A\left(P_{F=1\%}-dP\right)=\frac{C_0^A\left(P_{F=1\%}\right)}{\left(F^A\left(P_{F=1\%}-dP\right)-0.01\right)+D_0^A\left(P_{F=1\%}-dP\right)\cdot\left(1-F^A\left(P_{F=1\%}-dP\right)-0.01\right)} \quad \text{Eq. S-3}$$

$$C_0^A\left(P_{F=1\%}-2dP\right)=\frac{C_0^A\left(P_{F=1\%}-dP\right)-\left(F^A\left(P_{F=1\%}-dP\right)-0.01\right)\cdot Cl^A\left(P_{F=1\%}-dP\right)}{1-\left(F^A\left(P_{F=1\%}-dP\right)-0.01\right)} \quad \text{Eq. S-4}$$

F^A is the melting degree of the lithology A. The new $D_0{}^A$ is calculated using the phase assemblage obtained with pMELTS at $(P_{F=1\%} + dP)$ and $F^A(P_{F=1\%} + dP)$.

These expressions can be generalised for a given pressure P_i:

$$Cl^A\left(P_i\right)=\frac{C_0^A\left(P_i+dP\right)}{\left(F^A\left(P_i\right)-F^A\left(P_i+dP\right)\right)+D_0^A\left(P_i\right)\cdot\left(1-\left(F^A\left(P_i\right)-F^A\left(P_i+dP\right)\right)\right)} \quad \text{Eq. S-5}$$

$$C_0^A\left(P_i-dP\right)=\frac{C_0^A\left(P_i\right)-\left(F^A\left(P_i\right)-F^A\left(P_i+dP\right)\right)\cdot Cl^A\left(P_i\right)}{1-\left(F^A\left(P_i\right)-F^A\left(P_i+dP\right)\right)} \quad \text{Eq. S-6}$$

The pressure increment in the calculation was $dP = 0.01$ GPa.

Table S-1 Major[a], trace[b] element and isotopic compositions of G2, KLB-1, KG1, KG2 and Bulk1.

	G2[c]	KLB-1[d]	KG1[e]	KG2[e]	Bulk1[f]
SiO_2	50.05	44.48	47.0	46.2	45.04
TiO_2	1.97	0.16	0.78	0.57	0.34
Al_2O_3	15.76	3.59	9.75	7.69	4.81
FeO	9.35	8.10	9.77	9.22	8.23
MnO	0.17	0.12	0	0	0.13
MgO	7.90	39.22	23.6	28.8	36.09
CaO	11.74	3.44	7.35	6.05	4.27
Na_2O	3.04	0.30	1.52	1.11	0.57
K_2O	0.03	0.02	0.12	0.09	0.02
Ni	200	1964	1082	1376	1788
Rb	1.188	0.02	0.604	0.409	0.137
Ba	19.32	0.227	9.774	6.591	2.136
Th	0.135	0.004	0.070	0.048	0.017
U	0.046	0.0018	0.0239	0.0165	0.0062
Nb	6.13	0.0864	3.1082	2.1009	0.6908
Cla	2.695	0.134	1.415	0.988	0.390
Ce	8.161	0.421	4.291	3.001	1.195
Sr	98.11	6.092	52.101	36.765	15.294
Nd	8.375	0.483	4.429	3.114	1.272
Zr	65	4.269	34.635	24.513	10.342
Sm	2.3	0.21	1.26	0.91	0.42
Hf	1.709	0.127	0.918	0.654	0.285
Eu	1.055	0.086	0.571	0.409	0.183
Gd	3.7	0.324	2.012	1.449	0.662
Tb	0.7	0.064	0.382	0.276	0.128
Dy	4.4	0.471	2.436	1.781	0.864
Ho	1.15	0.108	0.629	0.455	0.212
Y	24.72	3.129	13.925	10.326	5.288
Er	2.653	0.329	1.491	1.104	0.561
Yb	3.4	0.348	1.874	1.365	0.653
Lu	0.371	0.056	0.214	0.161	0.088
$^{143}Nd/^{144}Nd$	0.5127	0.5134	0.512738	0.512819	0.512939
$^{87}Sr/^{86}Sr$	0.7037	0.7020	0.703636	0.703493	0.703306

[a] in wt. %
[b] in ppm
[c] G2: Major element composition is from Perterman and Hirschmann (2003); Ni content is from Sobolev *et al.* (2007); trace element composition corresponds to the composition K11 from Koorneff *et al.* (2012b); isotopic composition corresponds to a 2 Ga recycled oceanic crust altered by sea water and modified during the subduction process by dehydration using the model of Stracke *et al.* (2003).
[d] KLB-1: Major element composition and Ni content are from Hirose and Kushiro (1993); trace element composition is DDMM from Workman and Hart (2005); isotopic composition corresponds to the extreme D-MORB from Salters and Stracke (2004).
[e] KG1 and KG2: Major element compositions are from Kogiso *et al.* (1998); Ni content and trace element and isotopic compositions calculated as 1G2:1KLB-1 and 1G2:2KLB-1, respectively.
[f] Bulk1: Major, trace element and isotopic compositions are calculated as 1G2:9KLB-1.

Mineral–melt partition coefficients depend on the melt and mineral compositions (*e.g.*, Nielsen, 1988; Blundy and Wood, 1991), pressure and temperature conditions (*e.g.*, Taura *et al.*, 1998), oxygen fugacity (Laubier *et al.*, 2014), and consequently might differ for KLB-1, KG1, KG2 and G2 melts and from partition coefficients from Smith and Asimow (2005). However, the residual modal mineralogy exerts the major control on the bulk partition coefficient and consequently on the trace element composition of the melt. Because the residual mineralogy is adapted for each lithology during melting using pMELTS modelling, the use of constant partition coefficients in these calculations is not expected to introduce large errors.

(2) Accumulated melt.

Compositions of the accumulated melts are calculated for complete mixing of melts from the two mantle components integrated over the melting column. At P_i, the composition of the aggregated melt is:

$$\bar{Cl}(Pi) = \frac{\sum_{P_{F=1\%}}^{P_i} \phi_i^A \cdot M_i \cdot Cl^A(P_i) + \left(1-\phi_i^A\right) \cdot M_i \cdot Cl^B(P_i)}{\sum_{P_{F=1\%}}^{P_i} M_i} \quad \text{Eq. S-7}$$

with ϕ_i^A, the proportion of the oceanic crust formed at P_i and derived from lithology A such as:

$$\sum_{P_{F=1\%}}^{P_i} \phi_i^A = tc^{Pyr} / tc \quad \text{Eq. S-8}$$

with tc the thickness of the generated oceanic crust, tc^{Pyr}, the proportion of the crust derived from the pyroxenite component, and M_i, the proportion of oceanic crust formed between P_i and $P_i + dP$ such as:

$$\sum_{P_{F=1\%}}^{P_c} M_i = 100 \quad \text{Eq. S-9}$$

Olivine nickel content modelling

Contrary to the model proposed here, Herzberg *et al.* (2016) emphasised the lack of lithological variability in the Icelandic source based on olivine chemistry and in particular, on transition metal contents in olivine. Part of the disagreement is because a false dichotomy has been set up in which mantle lithologies are divided into two categories which are olivine-free lithologies (such as Px-1 or G2) and "normal" peridotite.

To test my model, I calculated the Fo and Ni contents of olivine produced during the low-pressure fractional crystallisation of the aggregated melts produced by the KG1-configuration and compared the results to Ni and Fo contents of olivines from Icelandic basalts (Fig. S-9; Sobolev *et al.*, 2007; Shorttle and Maclennan, 2011).

The starting Ni content of KLB-1 was taken from Hirose and Kushiro (1993). The starting Ni content of G2 was taken from Sobolev *et al.* (2005). KG1 Ni content was calculated using the 1:1 proportion between KLB-1 and G2 (Table S-1).

Because the trace element – isotope systematics of Icelandic basalts imply that melts are sampled at various depths along the melting column, I did calculations for three different melt compositions: the aggregated melt sampled at 4 GPa, where only KG1 is melting, the aggregated melt sampled at 1.5 GPa, and the aggregated melt sampled at the base of the crust, 0.6 GPa, where melting is assumed to stop. Ni contents of the aggregated melts were calculated in three steps: (1) I used Melt-PX to calculate the melting degree of KG1 and KLB-1 at 4, 1.5 and 0.6 GPa in the KG1-configuration (Table S-2) and I used pMELTS to calculate the residual mode for each lithology (Table S-2) at the corresponding *P-F* conditions (see above for details on Melt-PX and pMELTS calculations). (2) Because the Ni partition coefficient between olivine and melt is a function of temperature and/or pressure (Matzen *et al.*, 2013), in addition to composition (*e.g.*, Leeman and Lindstrom 1978; Beattie, 1993; Putirka *et al.* 2011; Matzen *et al.*, 2017), I used the Ni partitioning model of Matzen *et al.* (2017) to calculate the Ni content in melts derived from each lithology at the corresponding pressure. This model allows me to separate the effects of temperature from composition. Liquidus temperature and olivine composition in equilibrium with each melt (required to use Matzen *et al.*'s model) were calculated with the PRIMELT2.xls software (Herzberg and Asimow, 2008). Melts were run through PRIMELT2.xls assuming a major element composition of the mantle source equal to Bulk-1 (Table S-1). The oxidation state of the source was fixed at $Fe^{2+}/\sum Fe$ and Fe_2O_3 ratios of 0.89 and 0.5, respectively. The composition of the KG1- and KLB-1 derived melts used in the calculations are reported in Table S-2. (3) I calculated the Ni (and major element) contents in the aggregated melts according the contribution of each melt to the bulk magmatic productivity (*i.e.* Eq. S-8). Compositions of the aggregated melts used in the calculations are reported in Table S-3.

Table S-2 Melt compositions and parameters used in olivine fractionation modelling.

P	4 GPa	1.5 GPa		0.6 GPa	
	KG1[a]	KG1[b]	KLB-1[c]	KG1[b]	KLB-1[d]
SiO_2	43.0	49.9	48.6	49.9	50.7
TiO_2	3.32	0.45	1.16	0.45	0.42
Al_2O_3	15.5	13.8	14.3	13.8	14.6
FeO	11.5	7.92	9.19	7.92	7.64
MgO	14.2	15.7	13.5	15.7	13.4
CaO	7.82	10.7	10.2	10.7	11.2
Na_2O	3.68	1.04	2.65	1.04	1.50
K_2O	0.87	0.04	0.21	0.04	0.19
F[e]	2.0	48.5	16.4	71.0	23.0
X_{ol}[f]	20.8	11.5	59.5	29.0	70.7
X_{opx}[f]	1.8	17.5	16.6	0	5.5
X_{cpx}[f]	47.2	21.4	7.0	0	0.6
X_{gt}[f]	29.9	0	0	0	0
X_{sp}[f]	0.3	1.1	0.5	0	0.2
T_L[g]	1785	1712	1662	1667	1616
Fo[g]	88.3	92.0	90.1	92.3	91.5
$D_{Ni}^{ol/liq}$[h]	4.25	4.61	5.58	4.96	6.19
Ni in melt[i]	636	657	498	504	415

[a] Major-element composition used to model the KG1-derived melt at 4 GPa (glass in run #KH22 in Kogiso *et al.*, 1998).
[b] Major-element composition used to model the KG1-derived melt at 1.5 GPa and 0.6 GPa. GPa (glass in run #KH43 in Kogiso *et al.*, 1998).
[c] Major-element composition used to model the KBL-1-derived melt at 1.5 GPa (glass in run #20 in Hirose and Kushiro, 1993).
[d] Major-element composition used to model the KBL-1-derived melt at 0.6 GPa (glass in run #14 in Hirose and Kushiro, 1993).
[e] Melting degree calculated with Melt-PX at the corresponding pressure along the adiabatic path.
[f] Mode of the residual solid phases of each lithology at the corresponding pressure along the adiabatic path.
[g] Calculated liquidus temperature (T_L) in kelvin and forsterite content (Fo) of the olivine in equilibrium with each liquid at the corresponding pressure (Herzberg and Asimow, 2008).
[h] Calculated $D_{Ni}^{ol/liq}$ using the Ni partitioning model from Matsen *et al.* (2017).
[i] Ni content (in ppm) in the melts. Contents in melts from KG1 and KLB-1 are calcuated using the modelled $D_{Ni}^{ol/liq}$, and using Ni partitioning callibration for orthopyroxene-melt (Beattie *et al.*, 1991), olivine-garnet (Canil, 1999) and orthopyroxene-clinopyroxene (Seitz *et al.*, 1999).

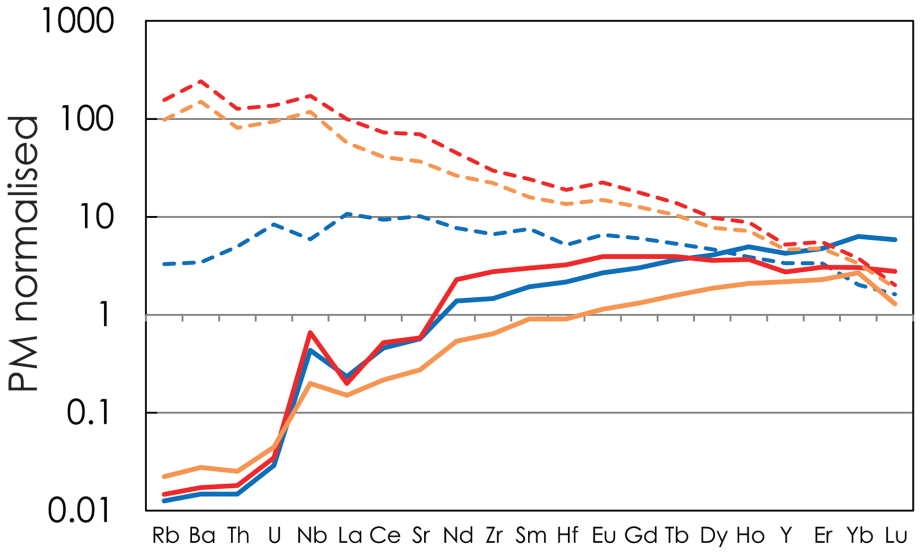

Figure S-5 Primitive mantle (PM; Sun and McDonough, 1989) normalised trace element patterns of the first degree melts (dashed lines) and the last accumulated melts produced at the base of the crust (solid lines) in G2- (red), KG1- (orange) and KG2- (blue) configurations.

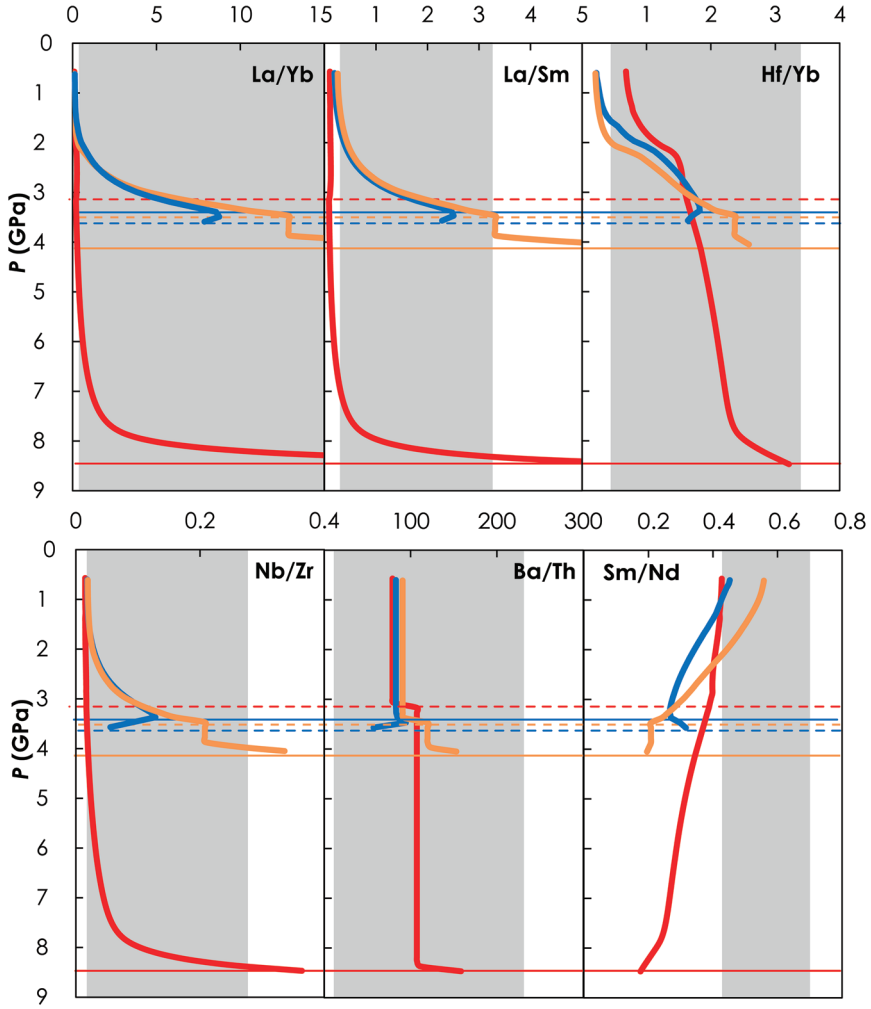

Figure S-6 Incompatible trace element ratios of the calculated accumulated melts as functions of the pressure in the three configurations (colour code is the same as in Fig. S-5). Solid lines represent the formation pressure of the first degree melt from the enriched mantle component (G2, KG1 or KG2) and dashed lines represent the formation pressure of the first degree melt from the peridotite component in the corresponding mantle configuration. The grey areas represent the range of compositional ratios in Icelandic basalts with MgO contents between 9.5 and 17 wt. % from the Northern Volcanic zone, the Reykjanes Peninsula, the Snaefellsnes area and the South Eastern Volcanic Zone (GEOROC).

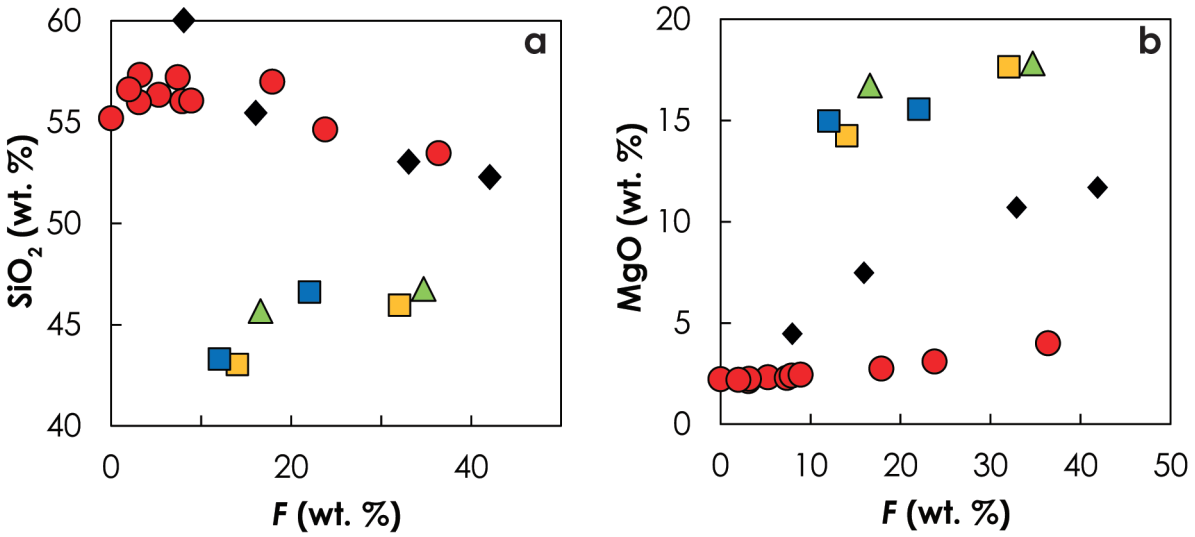

Figure S-7 Comparison of SiO_2 **(a)** and MgO **(b)** contents of the melt produced by G2 (red circles; Pertermann and Hirschmann, 2003), KG1 and KG2 (orange and blue squares, respectively; Kogiso *et al.,* 1998), Px-1 (black-diamond; Sobolev *et al*., 2007), and KLB-1 (green triangles; Hirose and Kushiro, 1993) at 3 GPa.

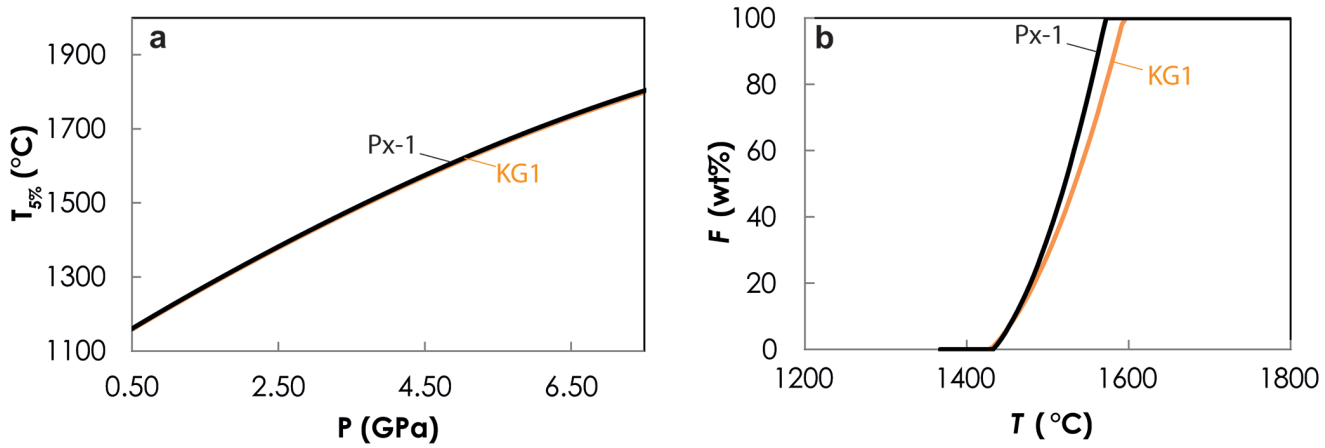

Figure S-8 Near-solidus curves ($T_{5\%}$) **(a)** and melting curves at 3 GPa **(b)** calculated using Melt-PX (Lambart *et al*., 2016) for Px-1 (black; Sobolev *et al*., 2007) and KG1 (orange; Kogiso *et al*., 1998) compositions.

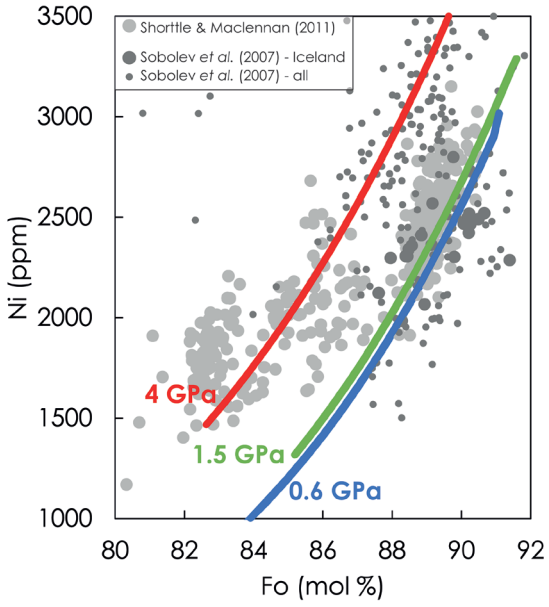

Figure S-9 Ni content of olivines from Icelandic basalts (large dark grey circles, Sobolev *et al.,* 2007; large light grey circles, Shorttle and Maclennan, 2011). The lines are modelled olivine compositions produced by fractionally crystallising aggregated parental melts sampled at 4, 1.5 and 0.6 GPa along the adiabatic path in the KG1-configuration. The melts chosen for modelling are reported in Table S-3. Parental melts then had equilibrium olivine fractionally extracted from them at 1 bar using olivine compositions calculated with PRIMELT2.xls (Herzberg and Asimow, 2008) and according the Ni partitioning model of Matzen *et al.* (2017). Data from Sobolev *et al.* (2007) in other locations are also shown for comparison (small dark grey circles). See text for details of calculations.

Table S-3 Compositions of the aggregated parental melt (APM) sampled at 4, 1.5 and 0.6 GPa and of the olivine in equilibrium at 1 bar.

	4 GPa	1.5 GPa	0.6 GPa
tc^{Pyr}/tc [a]	1	0.54	0.53
SiO_2 (wt. %)	43.0	49.2	49.5
TiO_2 (wt. %)	3.32	0.83	0.84
Al_2O_3 (wt. %)	15.5	14.1	14.4
FeO (wt. %)	11.5	8.61	8.52
MgO (wt. %)	14.2	14.5	13.5
CaO (wt. %)	7.82	10.4	10.6
Na_2O (wt. %)	3.68	1.90	2.16
K_2O (wt. %)	0.87	0.13	0.20
Ni (ppm)	636	571	468
T_L [b]	1601	1609	1586
Fo [b]	90.0	91.6	91.1
$D_{Ni}^{ol/liq}$ [c]	5.72	5.76	6.44
Ni in ol [d]	3641	3288	3016

[a] Contribution of the melt derived from KG1 to the volume of magma produced.
[b] Calculated liquidus temperature (T_L) and forsterite content (Fo) of the olivine in equilibrium with APM at 1 bar (Herzberg and Asimow, 2008).
[c] $D_{Ni}^{ol/liq}$ at 1 bar using Matzen *et al.* (2017) model
[d] Ni content (in ppm) in olivine in equilibrium with APM at 1 bar

Ni contents of the olivine that fractionates from the aggregated magmas at 1 bar were estimated using $D_{Ni}^{ol/liq}$ at 1 bar according Matzen *et al.*'s (2017) model (Fig. S-9); liquidus temperature of the aggregated melts and olivine composition in equilibrium at 1 bar were calculated with PRIMELTS2.xls using the same mantle source composition and oxidation state as above.

Most of the olivine Ni variation reported by Sobolev *et al.* (2007) and Shorttle and Maclennan (2011) can be explained by varying the sampling pressure of the aggregated melts in the melting column, with the compositions richest in Ni sampled at the highest pressure where the contribution of KG1 is the largest. Similar results were obtained by Shortlle and Maclennan (2011) using KG2- and KBL-1-derived melts. The authors also showed that fractionation of cpx and plagioclase in addition to olivine when melts reach 9 wt. % MgO could also explained the olivine compositions richest in Ni. However, the melting behaviours of the different lithologies present in the source were not taken into account. In particular, because KG2 starts to melt after the peridotite along the adiabatic path (Fig. S-3), the contribution of this lithology to the magma production cannot explain the trace element – isotope systematics of Icelandic basalts (Fig. 2e-f in the main text). In addition, calculations presented here consider the effect of pressure on Ni partitioning and support a model in which aggregated melts are collected at various pressures of the melting column.

Supplementary Information References

Beattie, P. (1993) Olivine-melt and orthopyroxene-melt equilibria. *Contributions to Mineralogy and Petrology* 115, 103–111.

Beattie, P., Ford, C., Russell, D. (1991) Partition coefficients for olivine-melt and orthopyroxene-melt systems. *Contributions to Mineralogy and Petrology* 109, 212–224.

Berman, R.G., Koziol, A.M. (1991) Ternary excess properties of grossular-pyropealmandine garnet and their influence in geothermobarometry. *American Mineralogist* 76, 1223–1231.

Blundy, J.D., Wood, B.J. (1991) Crystal-chemical controls on the partitioning of Sr and Ba between plagioclase feldspar, silicate melts and hydrothermal solutions. *Geochimica et Cosmochimica Acta* 55, 193–209.

Brown, E.L., Lesher, C.E. (2014) North Atlantic magmatism controlled by temperature, mantle composition and buoyancy. *Nature Geoscience* 7, 820–824.

Canil, D. (1999) The Ni-in-garnet geothermometer: calibration at natural abundances. *Contributions to Mineralogy and Petrology* 136, 140–246

Ghiorso, M.S., Hirschmann, M.M., Reiners, P.W., Kress, V.C.III (2002) The pMELTS: A revision of MELTS for improved calculation of phase relations and major element partitioning related to partial melting of the mantle to 3 GPa. *Geochemistry, Geophysics, Geosystems* 3, 1–35.

Hart, S.R., Blusztajn, J., Dick, H.J.B., Meyer, P.S., Muehlenbachs, K. (1999) The fingerprint of seawater circulation in a 500-meter section of oceanic crust gabbros. *Geochimica et Cosmochimica Acta* 63, 4059–4080.

Herzberg, C., Asimow, P.D. (2008) Petrology of some oceanic island basalts: PRIMELT2.XLS software for primary magma calculation. *Geochemistry, Geophysics Geosystems* 9, Q09001, doi:10.1029/2008GC002057.

Herzberg, C., Vidito, C., Starkey, N.A. (2016) Nickel-cobalt contents of olivine record origins of mantle peridotite and related rocks. *American Mineralogist* 101, 1952–1966.

Hirose, K., Kushiro, I. (1993) Partial melting of dry peridotites at high pressures: Determiantion of compositions of melts segregated from peridotite using aggregates of diamond. *Earth and Planetary Science Letters* 114, 477–489.

Kelemen, P.B., Hirth, G., Shimizu, N., Spiegelman, M., Dick, H.J.B. (1997) A review of melt migration processes in the adiabatically upwelling mantle beneath oceanic spreading ridges. *Philosophical Transactions of the Royal Society of London* A355, 282–318.

Klein, E.M., Langmuir, C.H. (1987) Global correlations of ocean ridge basalt chemistry with axial depth and crustal thickness. *Journal of Geophysical Research* 92, 8089–8115.

Kogiso, T., Hirose, K., Takahashi, E. (1998) Melting experiments on homogeneous mixtures of peridotite an.d basalt: application to the genesis of ocean island basalts. *Earth and Planetary Science Letters* 162, 45–61.

Koornneef, J.M., Stracke, A., Bourdon, B., Grönvold, K. (2012a) The influence of source heterogeneity on the U–Th–Pa–Ra disequilibria in post-glacial tholeiites from Iceland. *Geochemica et Cosmochemica Acta* 87, 243–266.

Koornneef, J.M., Stracke, A., Bourdon, B., Meier, M.A., Jochum, K.P., Stoll, B., Grönvold, K. (2012b) Melting of a Two-component Source beneath Iceland. *Journal of Petrology* 53, 127–157.

Lambart, S., Baker, M.B., Stolper, E.M. (2016) The role of pyroxenite in basalt genesis: Melt-PX, a melting parameterization for mantle pyroxenites between 0.9 and 5GPa. *Journal of Geophysical Research: Solid Earth* 121, doi:10.1002/2015JB012762.

Langmuir, C.H., Klein, E.M., Plank, T. (1992) Petrological systematics of mid-ocean ridge basalts: constraints on melt generation beneath ocean ridges. *American Geophysical Union Monographs* 71, 183–280.

Laubier, M., Grove, T.L., Langmuir, C.H. (2014) Trace element mineral/melt partitioning for basaltic and basaltic andesitic melts: An experimental and laser ICP-MS study with application to the oxidation state of mantle source regions. *Earth and Planetary Science Letters* 392, 265–278.

Leeman, W.P., Lindstrom, D.J. (1978) Partitioning of Ni^{2+} between basaltic and synthetic melts and olivines—an experimental study. *Geochimica et Cosmochimica Acta* 42, 801–816.

Maclennan, J., McKenzie, D., Hilton, F., Gronvöld, K., Shimizu, N. (2003) Geochemical variability in a single flow from northern Iceland. *Journal of Geophysical Research* 108(B1), 2007, doi:10.1029/2000JB000142, 2003.

Matzen, A.K., Baker, M.B., Beckett, J.R., Stolper, E.M. (2013) The temperature and pressure dependence of nickel partitioning between olivine and silicate melt. *Journal of Petrology* 54, 2521–2545.

Matzen, A.K., Baker, M.B., Beckett, J.R., Wood, B.J., Stolper, E.M. (2017) The effect of liquid composition on the partitioning of Ni between olivine and silicate melt. *Contributions to Mineralogy and Petrology* 172, doi:10.1007/s00410-016-1319-8.

Nielsen, R.L. (1988) A model for the simulation of the combined major and trace element liquid lines of descent. *Geochimica et Cosmochimica Acta* 52, 27–38.

Pertermann, M., Hirschmann, M.M. (2003) Anhydrous Partial Melting Experiments on MORB-like Eclogite: Phase Relations, Phase Compositions and Mineral–Melt Partitioning of Major Elements at 2–3 GPa. *Journal of Petrology* 44, 2173–2201.

Phipps Morgan, J. (2001) Thermodynamics of pressure release melting of a veined plum pudding mantle. *Geochemistry, Geophysics, Geosystems* 2, 1001, doi:10.1029/2000GC000049.

Putirka, K., Ryerson, F.J., Perfit, M., Ridley, W.I. (2011) Mineralogy and composition of the oceanic mantle. *Journal of Petrology* 52, 279–313.

Salters, V.J.M., Stracke, A. (2004) Composition of the depleted mantle. *Geochemistry, Geophysics, Geosystems* 5, Q05004, doi:10.1029/2003GC000597.

Seitz, H.M., Altherr, R., Ludwig, T. (1999) Partitioning of transition elements between orthopyroxene and clinopyroxene in peridotitic and websteritic xenoliths: New empirical geothermometers. *Geochimica et Cosmochimica Acta* 63, 3967–3982.

Smith, P.M., Asimow, P.D. (2005) Adiabat_1ph: A new public front-end to the MELTS, pMELTS, and pHMELTS models. *Geochemistry, Geophysics, Geosystems* 6, Q02004, doi:10.1029/2004GC000816.

Shorttle, O., Maclennan, J. (2011) Compositional trends of Icelandic basalts: Implications for short–length scale lithological heterogeneity in mantle plumes. *Geochemistry, Geophysics, Geosystems* 12, Q11008, doi:10.1029/2011GC003748.

Shorttle, O., Maclennan, J., Lambart, S. (2014) Quantifying lithological variability in the mantle. *Earth and Planetary Science Letters* 395, 24–40.

Sobolev, A.V., Hofmann, A.W., Kuzmin, D.V., Yaxley, G.M., Arndt, N.T., Chung, S.L., Danyushevsky, L.V., Elliott, T., Frey, F.A., Garcia, M.O., Gurenko, A.A., Kamenetsky, V.S., Kerr, A.C., Krivolutskaya, N.A., Matvienkov, V.V., Nikogosian, I.K., Rocholl, A., Sigurdsson, I.A., Sushchevskaya, N.M., Teklay, M. (2007) The amount of recycled crust in sources of mantle-derived melts. *Science* 316, 412–417.

Sobolev, A.V., Hofmann, A.W., Sobolev, S.V., Nikogosian, I.K. (2005) An olivine-free mantle source of Hawaiian shield basalts, *Nature* 434, 412–417.

Stracke, A., Bizimis M., Salters V.J.M. (2003) Recycling oceanic crust: Quantitative constraints. *Geochemistry, Geophysics, Geosystems* 4, 8003, doi:10.1029/2001GC000223.

Sun, S.-S., McDonough, W.F. (1989) Chemical and isotopic systematics of oceanic basalts: implications for mantle composition and processes. *Geological Society, London, Special Publications* 42, 313–345.

Sun, W., Hu,Y., Kamenetsky, V.S., Eggins, S.M., Chen, M., Arculus, R.J. (2008) Constancy of Nb/U in the mantle revisited. *Geochimica et Cosmochimica Acta* 72, 3542–3549.

Taura, H., Yurimoto, H., Kurita, K., Sueno, S. (1998) Pressure dependence on partition coefficients for trace elements between olivine and the coexisting melts. *Physics and Chemistry of Minerals* 25, 469–484.

White, R.S., McKenzie, D. O'Nions, K (1992) Oceanic crustal thickness from seismic measurements and rare earth element inversions. *Journal of Geophysical Research* 97(B13), 19683–19715.

Weatherley, S.M., Katz, R.F. (2016) Melt transport in heterogeneous mantle beneath mid-ocean ridges. *Geochemica et Cosmochemica Acta* 172, 39–54.

Workman, R.K., Hart, S.R. (2005) Major and trace element composition of the depleted MORB mantle (DMM). *Earth and Planetary Science Letters* 231, 53–72.